

Scintillation of liquid neon from electronic and nuclear recoils

J. A. Nikkel,* R. Hasty, W. H. Lippincott, and D. N. McKinsey

Yale University, New Haven, CT

(Dated: November 27, 2006)

We have measured the time dependence of scintillation light from electronic and nuclear recoils in liquid neon, finding a slow time constant of $15.4 \pm 0.2 \mu\text{s}$. Pulse shape discrimination is investigated as a means of identifying event type in liquid neon. Finally, the nuclear recoil scintillation efficiency is measured to be 0.26 ± 0.03 for 387 keV nuclear recoils.

INTRODUCTION

Liquid neon has been suggested as a low-background scintillation medium for the CLEAN (Cryogenic Low Energy Astrophysics with Noble gases) experiment, which will have simultaneous sensitivity to both low energy solar neutrinos and WIMPs [1–3]. The CLEAN detector will use approximately 100 tonnes of liquid neon surrounded by photomultiplier tubes (PMTs) in a spherical geometry. Scintillation light resulting from both electronic and nuclear recoils will be detected by these PMTs. Liquid neon is a good candidate for low background experiments because it has no long lived radioactive isotopes, is easily purified, and is dense enough to allow for self-shielding, effectively eliminating backgrounds in the center of the detector. The solar neutrino signal will consist of electronic recoils, while a WIMP signal will consist of nuclear recoils. The physics goals of CLEAN require a method of discriminating between these two types of events.

It was pointed out in Ref. [2] and [3] that electronic and nuclear recoil events in liquid neon might be distinguished through the use of pulse shape discrimination (PSD). Interactions of ionizing radiation with liquid noble gases produce excimers that can exist in either a singlet or triplet state. The lifetime of the triplet state in liquid neon has been previously measured to be $3.9 \mu\text{s}$ [4]. The singlet lifetime is expected to be much shorter, on the order of a few nanoseconds, based on measurements of other liquid noble gases [5].

The slow scintillation light emitted by triplet molecules is suppressed in intensity by destructive triplet interactions, primarily Penning ionization and electron-triplet spin exchange; these reactions are stronger for higher excitation densities such as those produced by nuclear recoils. For a given event, measurement of the fraction of the total scintillation signal that is in the fast component can be used to determine which type of event has occurred.

PSD has also been studied in detail for liquid xenon based experiments [6, 7] and can be used to suppress gamma ray backgrounds. PSD in liquid helium has also been studied in order to separate electronic recoil events from ${}^3\text{He}(n,p){}^3\text{H}$ events in the search for the neutron electric dipole moment [8]. In an extension of the CLEAN

concept, PSD has been also suggested to counter ${}^{39}\text{Ar}$ background in single phase liquid argon dark matter detectors [9]. Previous measurements of liquid and solid neon [4] have compared beta induced scintillation to 5 MeV alpha induced scintillation, but no studies exist of PSD for the nuclear recoils characteristic of a WIMP signal.

Because the WIMP-nucleon scattering rate is expected to decay exponentially with nuclear recoil energy, the sensitivity of experiments to WIMPs depends crucially on energy threshold, which in turn depends both on the scintillation yield for nuclear recoils and the light detection efficiency of the apparatus. The scintillation yield from nuclear recoils relative to that from electronic recoils has been measured recently by several groups for liquid xenon [6, 10–12]. In contrast, the scintillation yield for nuclear recoils in liquid neon has not been measured.

In this paper we describe measurements of the pulse shape discrimination efficiency, nuclear recoil scintillation efficiency, and time dependence of liquid neon scintillation.

EXPERIMENTAL DETAILS

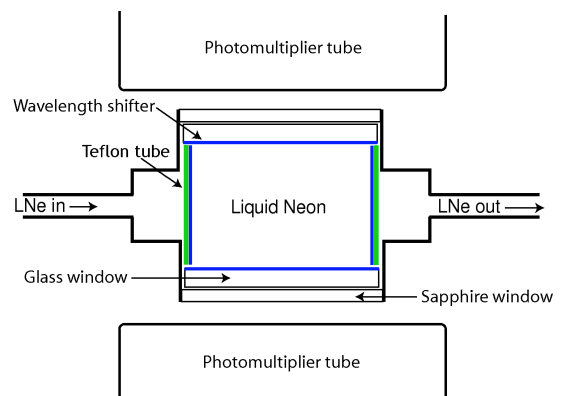


FIG. 1: Schematic representation of the scintillation cell.

The data presented here were obtained using a 200 ml scintillation vessel viewed by two 75 mm diameter photo-

multiplier tubes (PMTs) [17]. A schematic of the setup can be seen in Fig. 1.

The scintillation vessel is a stainless steel body attached to two titanium flanges into which 50 mm diameter sapphire windows are bonded with Stycast 2850 epoxy. Titanium and sapphire were chosen due to their similar thermal expansion coefficients, allowing a leak-tight seal when filled with liquid neon. Because liquid neon scintillates in the ultraviolet (≈ 77 nm) [13], we place inside the vessel secondary windows coated with a thin film of tetraphenyl butadiene (TPB [14]). The TPB shifts the wavelength of the ultraviolet light to approximately 440 nm so that it may pass through the windows and be detected by the PMTs. The top window is coated with 0.29 mg/cm² of TPB and the bottom window with 0.18 mg/cm². The inside wall of the vessel is lined with a PTFE sheet that is coated on the inner surface with 0.16 mg/cm² of TPB.

The scintillation vessel is housed inside a vacuum dewar for thermal insulation, and liquid neon is introduced through a tube on the side of the scintillation vessel. The neon is liquefied from purified gas in a copper can mounted to the end of a pulse-tube refrigerator [18]. All components that come into contact with the gas or liquid are baked to at least 60 C for 12 hours, and the ultra-high purity neon gas (99.999%) is passed through a heated gas purification getter [19] before it is liquefied.

A stainless steel tube leading out of the scintillation vessel leads to a charcoal trap connected in line. Purification of neon with charcoal using this method has been previously discussed in Ref. [15]. After the cell is filled with liquid, a small heater below the trap is energized, forcing vaporized neon through the charcoal and back into the liquefaction can. By monitoring the heat load on the refrigerator we calculate that a continuous flow rate of approximately 0.5 gas litres per minute was obtained over the course of the experiment.

Two sample oscilloscope traces from scintillation events in liquid neon can be seen in Fig. 2. The signal from each PMT is divided three ways with a linear fan-out. One copy goes to the triggering electronics and two copies go directly to an oscilloscope where they are digitized at two different gain settings. We use this technique to increase the effective dynamic range of the 8-bit oscilloscope digitization. The triggering electronics require a coincidence of at least one half of a photoelectron (pe) within 100 ns in each PMT.

All data analysis is performed in software. The first analysis step is to take collections of runs, typically two hours long, and find the value of the single photoelectron signal. For all types of excitations in the neon, there is a significant triplet component, and since this is spread out over many μ s, a large number of single photo-electron events can be analyzed to obtain the gain of the PMTs.

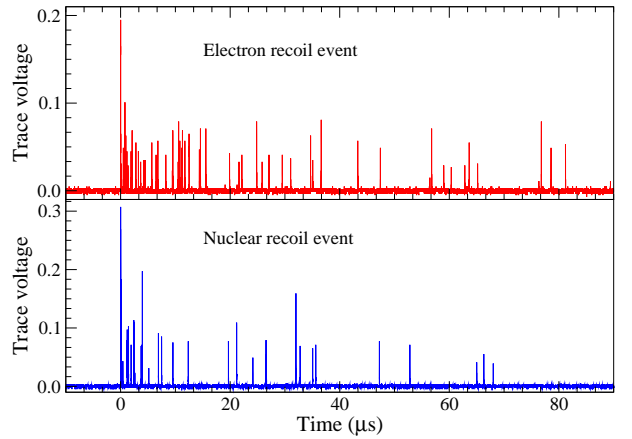


FIG. 2: Examples of two events that are identified as electronic and nuclear recoils using pulse shape discrimination. The discrimination method used is described in the Experimental Results section.

Sodium-22 Calibration

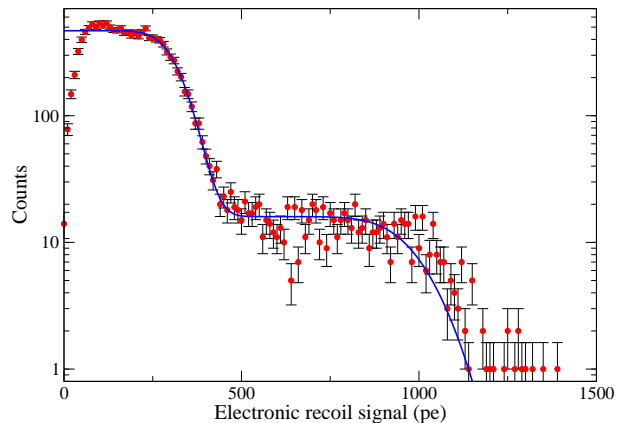


FIG. 3: Plot of ^{22}Na calibration data with fit to Eq. (1), indicating a detector signal yield of 0.93 ± 0.07 photoelectrons per keV.

We use a 10 μCi sealed ^{22}Na source to determine the absolute signal yield for electronic recoils. This source is placed on the outside of the vacuum enclosure to provide a source of high energy gamma rays. Because the gammas from this source are produced in the $e^+ + e^- \rightarrow \gamma + \gamma$ reaction, we can significantly reduce backgrounds due to other radioactive decays, as well as cosmic rays, by requiring a coincidence between the scintillation vessel and an external organic scintillation detector. The majority of the 511 keV gamma rays that interact in the neon Compton scatter, providing a wide range of energy depositions over the region of experimental interest. We also use these ‘tagged’ events for measuring the electronic recoil time dependence.

Data are analyzed from the two PMTs with the only

requirement that the integrated signal from one PMT be within a factor of four of the other. We fit the calibration data to a function that is comprised of two Gaussian-broadened step-functions,

$$N = A \left[1 - \operatorname{erf} \left(\frac{E - E_{511}}{\sigma_1 \sqrt{2}} \right) \right] + B \left[1 - \operatorname{erf} \left(\frac{E - E_{1274}}{\sigma_2 \sqrt{2}} \right) \right], \quad (1)$$

where $E = x/Y$ is the energy, Y is the yield, E_{511} is the value of the 511 keV Compton edge (341 keV) and E_{1274} is the value of the 1274 keV Compton edge (1062 keV). σ_1 and $\sigma_2 (= \sigma_1 \sqrt{E_{511}/E_{1274}})$ are the widths, and A and B are the relative sizes of the steps. The calibration data are shown in Fig. 3 along with a four parameter fit for σ_1 , A , B , and Y . From this fit, we have determined that the signal yield for electronic recoils in this detector is 0.93 ± 0.07 pe/keV at 511 keV.

We measured the stability of the system by taking individual ^{22}Na runs over the course of four days. We found that the signal yield remained constant to within 7%.

Nuclear recoils

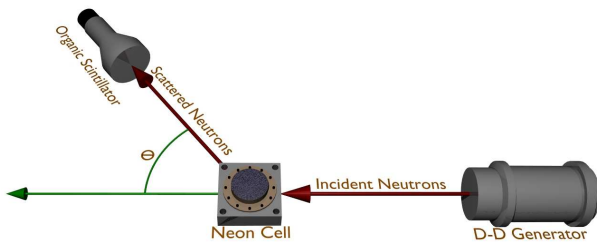


FIG. 4: Schematic of the neutron scattering setup.

To investigate the detector response to nuclear recoils, we use a portable deuterium-deuterium neutron generator [20] as a source and an organic scintillator as a secondary detector. The experimental setup can be seen schematically in Fig. 4. The nuclear recoil energy, E_{rec} , may be determined from the angle of the scattered neutron through simple kinematics,

$$E_{rec} = \frac{2E_{in}}{(1+M)^2} \left[1 + M - \cos^2(\theta) - \cos(\theta) \sqrt{M^2 + \cos^2(\theta) - 1} \right], \quad (2)$$

where E_{in} is the incident neutron energy (2.8 MeV), M is the atomic mass (20.18 for neon), and θ is the scattering angle of the outgoing neutron.

EXPERIMENTAL RESULTS

Pulse shape discrimination

To discriminate between electronic recoil and nuclear recoil events, we calculate f_{prompt} , the fraction of the signal that arrives in the first 100 ns.

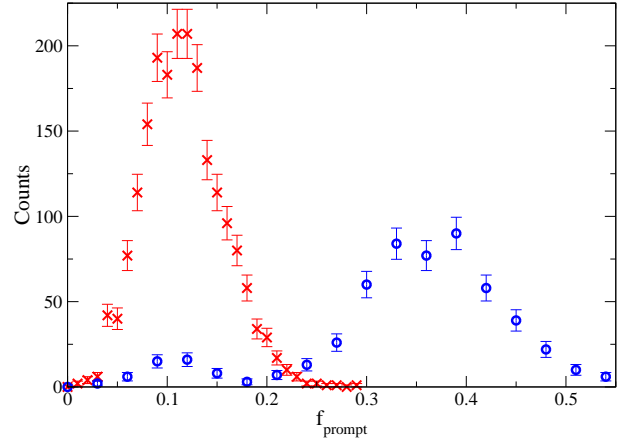


FIG. 5: Plot of the fraction of light in the prompt component (f_{prompt}) for electronic recoils (Xs) and electronic plus nuclear recoils (circles). Events are selected to be between 80 and 120 photoelectrons for this plot.

Figure 5 is a histogram of f_{prompt} for 1434 events identified as electronic recoils and 573 events identified as nuclear recoils. All events are selected to be between 80 and 120 photoelectrons. As one can see, there is a natural division at about $f_{prompt} = 0.25$. Using a 50% nuclear recoil acceptance ($f_{prompt} \geq 0.35$) we conclude that the discrimination efficiency exceeds one part in 1434.

There is a small population of events in the nuclear recoil set that have a small f_{prompt} . The neutron generator produces a large number of gamma rays, and some of those are misidentified by the time of flight cuts.

Time dependence

We estimate the temporal probability density functions for nuclear and electronic recoil events in liquid neon based on the data from events that yield between 80 and 120 photoelectrons. Because the d-d neutron generator emits significant numbers of gamma rays, we require that the fraction of light within the first 100 ns (f_{prompt}) be greater than 0.18 before it is considered to be a nuclear recoil. There is a clear separation in the neutron and gamma populations in Fig. 5 that justifies this cut. Additionally, a 100 ns window in the time of flight spectrum is allowed in order to reduce the number of gamma ray events in the region of interest. No such cuts are used for the tagged ^{22}Na electronic recoil events.

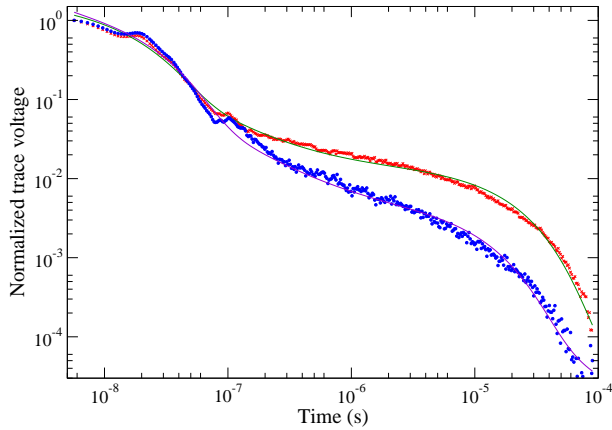


FIG. 6: Plot of the probability density function as a function of time for both electronic recoils (top curve) and nuclear recoils (bottom curve). Solid lines are fits described in the text.

For each event class, the trigger time is defined as the time that the voltage rises above 20% of its maximum value. These aligned pulses are averaged and then normalized in order to more easily compare them. Both gamma and neutron data are simultaneously fit using a least squares method to the following function,

$$p_m = Ae^{-(t-t_0)/\tau_1} + \frac{B}{t-t_0} + Ce^{-(t-t_0)/\tau_2}, \quad (3)$$

while allowing A , B , and C to vary between the two different types of excitations.

This function was constructed as an extension of the two exponential fit that one needs as a minimal description of the singlet and triplet decay constants for the neon molecules. The quality of fit to the neon data is statistically better with this hybrid function than it is with either a two or three term exponential fit function. The motivation for adding the $1/t$ term is based on observations of radiative decay in liquid helium scintillations [16] where the non-exponential component is explained as a two-body reaction effect. The resulting fit parameters are listed in Table I. We find the slow time constant to be significantly longer than that measured by Michniak *et al.* [4] ($15.4 \pm 0.2 \mu\text{s}$ vs. $3.9 \pm 0.5 \mu\text{s}$). We attribute this discrepancy to our continuous purification procedure which reduces impurities that may quench the triplet molecules.

The singlet decay time can not be directly calculated from τ_1 as the speed of the prompt pulse is also determined by the PMT timing and TPB wavelength shifter lifetime.

Parameter	Electronic recoils	Nuclear recoils
A	0.86 ± 0.16	1.33 ± 0.13
B (ns)	5.0 ± 0.2	3.78 ± 0.08
C	0.0137 ± 0.0004	0.00230 ± 0.00002
t_0 (ns)	-4.8 ± 0.9	
τ_1 (ns)	18.6 ± 0.2	
τ_2 (μs)	15.4 ± 0.2	

TABLE I: Fit parameters to Eq. (3) for both electronic and nuclear recoil events between 80 and 120 photoelectrons.

Nuclear recoil scintillation efficiency

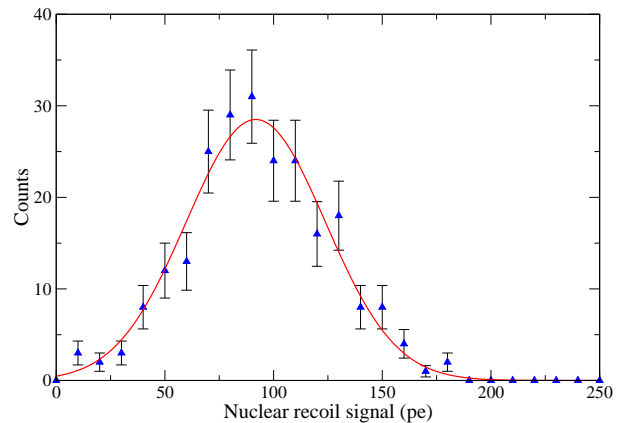


FIG. 7: Plot of the light production for 387 keV nuclear recoils with Gaussian fit.

The relative nuclear recoil scintillation efficiency is the ratio of light produced by nuclear recoils compared to that produced by electronic recoils of the same energy. For simplicity we assume that the electronic recoil scintillation efficiency is constant over our region of interest.

We choose a scattering angle of $120^\circ \pm 3^\circ$ which corresponds to a nuclear recoil energy deposition of 387 ± 11 keV. We exclude events from the raw data set that lie outside of a 60 ns time of flight window. The resulting data are plotted in Fig. 7.

The Gaussian best fit parameters yield a peak at 93 ± 2 photoelectrons and a width of 33 ± 3 photoelectrons. Therefore, the nuclear recoil signal yield is 0.24 ± 0.01 photoelectrons per keV. Using 0.93 ± 0.07 pe/keV for 511 keV electronic recoils, the relative nuclear recoil scintillation efficiency is 0.26 ± 0.03 at 387 ± 11 keV.

CONCLUSION

We have measured the time dependence of electronic and nuclear recoil scintillation events in liquid neon. We find that the slow time constant is $15.4 \pm 0.2 \mu\text{s}$ and find evidence for a $1/t$ term through least squares fitting. We

have also found that in our apparatus the signal yield for 511 keV electronic recoils is 0.93 ± 0.07 pe/keV and for 387 keV nuclear recoils is 0.24 ± 0.01 pe/keV. This implies a relative scintillation efficiency of 0.26 ± 0.03 at this energy. For a signal yield between 80 and 120 photoelectrons we find the pulse shape discrimination between nuclear and electronic recoils to be better than 1 part in 1434 with 50% nuclear recoil acceptance.

* Electronic address: james.nikkel@yale.edu

- [1] D. N. McKinsey and J. M. Doyle, *Journal of Low Temperature Physics* **118**, 153 (2000).
- [2] D. N. McKinsey and K. J. Coakley, *Astroparticle Physics* **22**, 355 (2005).
- [3] M. Boulay, A. Hime, and J. Lidgard, *Nuclear Physics B - Proceedings Supplements* **143**, 486 (2005).
- [4] R. A. Michniak, R. Alleaume, D. N. McKinsey, and J. M. Doyle, *Nuclear Instruments & Methods in Physics Research Section A-Accelerators Spectrometers Detectors and Associated Equipment* **482**, 387 (2002).
- [5] A. Hitachi, T. Takahashi, N. Funayama, K. Masuda, J. Kikuchi, and T. Doke, *Physical Review B* **27**, 5279 (1983).
- [6] D. Akimov, A. Bewick, D. Davidge, J. Dawson, A. S. Howard, I. Ivaniouchenkov, W. G. Jones, J. Joshi, V. A. Kudryavtsev, and T. B. Lawson, *Physics Letters B* **524**, 245 (2002).
- [7] G. Davies, J. Davies, J. Lewin, P. Smith, and W. Jones, *Physics Letters B* **320**, 395 (1994).
- [8] R. Golub and S. K. Lamoreaux, *Physics Reports* **237**, 1 (1994).
- [9] M. Boulay and A. Hime, *Astroparticle Physics* **In Press**, **Corrected Proof**, (2006).
- [10] F. Arneodo, B. Baiboussinov, A. Badertscher, P. Benetti, E. Bernardini, A. Bettini, A. Borio di Tiogliole, R. Brunetti, A. Bueno, and E. Calligarich, *Nuclear Instruments and Methods in Physics Research Section A: Accelerators, Spectrometers, Detectors and Associated Equipment* **449**, 147 (2000).
- [11] E. Aprile, K. L. Giboni, P. Majewski, K. Ni, M. Yamashita, R. Hasty, A. Manzur, and D. N. McKinsey, *Physical Review D* **72**, 72006 (2005).
- [12] V. Chepel, V. Solovov, F. Neves, A. Pereira, P. J. Mendes, C. P. Silva, A. Lindote, J. P. da Cunha, M. I. Lopes, and S. Kossionides, *Scintillation efficiency of liquid xenon for nuclear recoils with the energy down to 5 keV* (2006).
- [13] R. E. Packard, F. Reif, and C. M. Surko, *Phys. Rev. Lett.* **25**, 1435 (1970).
- [14] D. N. McKinsey, C. R. Brome, J. S. Butterworth, R. Golub, K. Habicht, P. R. Huffman, S. K. Lamoreaux, C. E. H. Mattoni, and J. M. Doyle, *Nuclear Instruments & Methods in Physics Research Section B-Beam Interactions with Materials and Atoms* **132**, 351 (1997).
- [15] M. K. Harrison, W. H. Lippincott, D. N. McKinsey, and J. A. Nikkel, *Nuclear Instruments and Methods in Physics Research A* doi:[10.1016/j.nima.2006.10.135](https://doi.org/10.1016/j.nima.2006.10.135) (2006).
- [16] D. N. McKinsey, C. R. Brome, J. S. Butterworth, S. N. Dzhosyuk, P. R. Huffman, C. E. H. Mattoni, J. M. Doyle, R. Golub, and K. Habicht, *Physical Review A* **59**, 200 (1999).
- [17] Electrontubes model D746, www.electrontubes.com
- [18] Cryomech model PT805, www.cryomech.com
- [19] Omni Nupure III, www.nupure.com
- [20] Themo Electron Model MP320, www.thermo.com